JOURNAL OF MATERIALS SCIENCE **37** (2002) 1523–1533

Transformation properties and microstructure of sputter-deposited Ni-Ti shape memory alloy thin films

T. LEHNERT*,‡, S. CREVOISERAT, R. GOTTHARDT
Institut de Physique de la Matière Complexe, Faculté des Sciences de Base, Ecole Polytechnique Fédérale de Lausanne (EPFL), 1015-Lausanne, Switzerland
E-mail: Thomas.Lehnert@epfl.ch

The influence of annealing parameters on the martensitic phase transformation in sputter-deposited Ti rich Ni-Ti films is systematically studied by differential scanning calorimetry and by transmission electron microscopy. The annealing temperature range extends from the crystallization temperature of the films up to 900°C. For increasing temperature, multiple phase transformations, transformations via an R-phase or direct martensite/austenite transformations are observed. A similar behavior is found for increasing annealing time. Related changes of the film microstructure, such as the strongly varying distribution of round Ti_2Ni precipitates in the grains, are analyzed. Transformation temperatures could be shifted over a wide range by adjusting the film composition from 48 to 54 at.% Ti. The corresponding transformation curves, grain structure as well as nature and amount of precipitates were investigated. No subsequent annealing process is required for films deposited on substrates heated above about 500°C. In this case, the as-deposited films have a very fine-grained and homogeneous microstructure.
© *2002 Kluwer Academic Publishers*

1. Introduction

Sputter-deposited Ni-Ti thin films showing a martensitic phase transformation and the related shape memory effect (SME) become increasingly important in the field of the development of new microactuators and devices, such as microvalves or moving cantilevers for microgrippers or optical switches [1–3]. Films with a thickness of only a few microns allow a high degree of miniaturization. The specific work power of shape memory alloy (SMA) devices is expected to exceed clearly the values achievable with other types of actuators as weight and dimensions become very small [4]. Due to the mechanical strength of these films, not only on-wafer designs, but also free-standing films can be employed. New local heat treatments may be applied to these thin films, opening the way to a new class of monolithic devices [5, 6]. Control of transformation temperatures and mechanical properties by suitable thermal treatments is an important issue. In this context, it is necessary to investigate the film microstructure in detail. The study of precipitates in the material is of particular interest because of the strong effect they may have on the film properties [7]. A recent overview of the present status of the Ni-Ti thin film development can be found in [8] and references therein.

Another interesting aspect of sputter-deposited films is that their thickness can be easily reduced to submicron dimensions. Therefore thin films are well-suited to investigate a possible size effect on the martensitic transformation [9]. Because of its high sensitivity, nuclear magnetic resonance (NMR) spectroscopy is a suitable tool to study this effect [10]. For this kind of investigation method, it is also indispensable to know the nature and the amount of precipitates present in the film.

In order to be able to control film fabrication for such different purposes and to adjust the required transformation parameters, the effect of annealing temperature, annealing time, substrate temperature and target composition was investigated in this paper. The goal of this paper was to carry out a systematic study of the martensitic transformation behavior and of the corresponding microstructure of the films at the same time. This relationship is not clearly investigated in literature so far. The transformation is displayed by differential scanning calorimetry (DSC). The microstructure was investigated by transmission electron microscopy (TEM).

2. Thin film fabrication process

The films are fabricated by RF magnetron sputter deposition (Ar gas at 6.7×10^{-3} mbar, background pressure

*Author to whom all correspondence should be addressed.
‡*Present Address*: Institut de Microélectronique et de Microsystème, Faculté des Sciences et Techniques de l'Ingénieur, Ecole Polytechnique Fédérale de Lausanne, CH - 1015 Lausanne, Switzerland.

$<5 \times 10^{-7}$ mbar). Two 2-inch water-cooled and individually powered Ni-Ti targets can be used simultaneously. Two different materials have been employed (material I 49.6 at.% Ti, material II 50.6 at.% Ti).

The amount of Ti in the sputter-deposited films was found to be about 2 at.% lower than in the pure Ni-Ti targets. Effects arising from changing target surface topography during sputtering or capture of Ti by reactive contaminations in the vacuum chamber were outlined as possible explanations [11]. In order to compensate for the Ti loss and to adjust different film compositions, 2 to 6 pellets of pure Ti were incorporated in the targets. Co-sputtering of two targets with a typical power density of 6.1 W/cm^2 results in a deposition rate of 1.4 μm/h. Fine adjustment of the film composition can be achieved by using simultaneously two differently enriched targets and by varying the individual power level for each cathode. Most of the film samples investigated in this paper are Ti rich.

Films were generally deposited on unheated glass substrates fixed on a rotating substrate mount for better homogeneity. The adhesion on glass is sufficiently low so that they can easily be peeled off. Free standing films are required for the calorimetric characterization but also for certain applications in microengineering. For the DSC measurements a film sample mass of typically 3 mg was sufficient to obtain a good signal to noise ratio. The as-deposited films are amorphous and require subsequent annealing for crystallization. For that purpose, the samples were encapsulated in an evacuated and Ar filled quartz tube. A single annealing step was carried out. A comparison with films deposited on heated Si/SiO_2 substrates will also be presented.

Uniformity of a Ni-Ti film sample of typical size (2×2 cm^2) was checked by means of a current stabilized electron microprobe. A maximum radial variation of 0.1 ± 0.07 at.% Ti per cm was found. Composition non-uniformity is therefore not considered as an important issue for the experiments presented in this paper.

The absolute composition of films and targets was determined by EDS measurements in a Philips XL30 scanning electron microscope (EDAX, ZAF standardless quantification, $V = 15$ kV). Calibration was carried out with a Ni-Ti sample of known composition. Due to systematic errors, an accuracy of ± 0.5 at.% is estimated for the absolute composition values.

3. DSC crystallization curves

In order to determine the crystallization temperature range of the amorphous as-deposited Ni-Ti films, the heat flow during heating up to 550°C was measured by DSC (heating rate 10°C/min). Fig. 1 shows the curve of a Ni-Ti film with nearly equiatomic composition (material I). A clear exothermic crystallization peak appears at 462°C. The corresponding enthalpy is 31 ± 1 J/g. Comparing all samples in the composition range from 48 to 54 at.% Ti, crystallization temperatures fluctuated between 460°C and 490°C but no systematic shift was found.

In the DSC curve of Fig. 1 a very broad structure appears in the temperature range between 200°C and 400°C. The origin of this feature is probably due to a relaxation of the amorphous as-deposited film structure [12]. Selected area diffraction (SAD) patterns taken in the as-deposited film and after annealing at 330°C are identical and correspond to an amorphous phase. It is interesting to mention that in multilayers of subsequently superposed Ti and Ni layers an amorphization reaction of the initially crystallized multilayer structure takes place in this temperature range [13, 14].

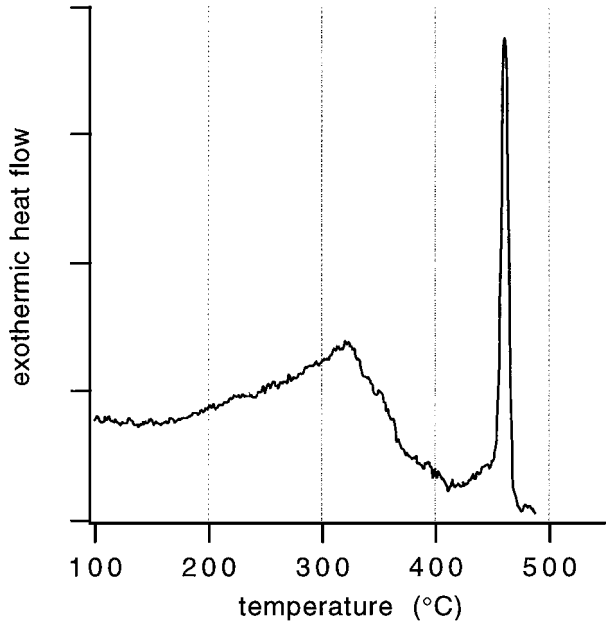

Figure 1 DSC crystallization curve of a Ni-Ti film.

4. Film properties as a function of annealing temperature

4.1. DSC curves

The martensitic phase transformation in the film samples was investigated by DSC after annealing at temperatures in the range of 450°C to 900°C for 30 min (water-quenched). All samples for this series were taken from the same piece of film (material I, thickness 8 μm, 50.4 at.% Ti). Fig. 2a and b show the corresponding DSC heating and cooling curves (rate 10°C/min, normalized with respect to mass). A complete thermal cycle was carried out before these DSC curves have been recorded.

In the temperature range close to the crystallization temperature, i.e. between 450°C and 500°C, DSC heating and cooling curves show weak peaks superposed on a strongly smeared out background signal. No distinct transformation temperature can be determined. At higher annealing temperatures, peaks become better defined. After annealing at 600°C and 700°C still several peaks appear in the DSC heating curves. They can be attributed to multiple martensite/austenite transformations at different temperatures, probably via an R-phase. In the corresponding cooling curves a peak at 56 ± 1°C, followed by a very broad structure extending to below 0°C, is observed. The transformation behavior of the sample annealed at 600°C was analyzed in more detail. For that purpose several partial thermal cycles covering different temperature ranges between -50°C and 100°C were carried out. This procedure reveals corresponding transformation peaks in the DSC heating

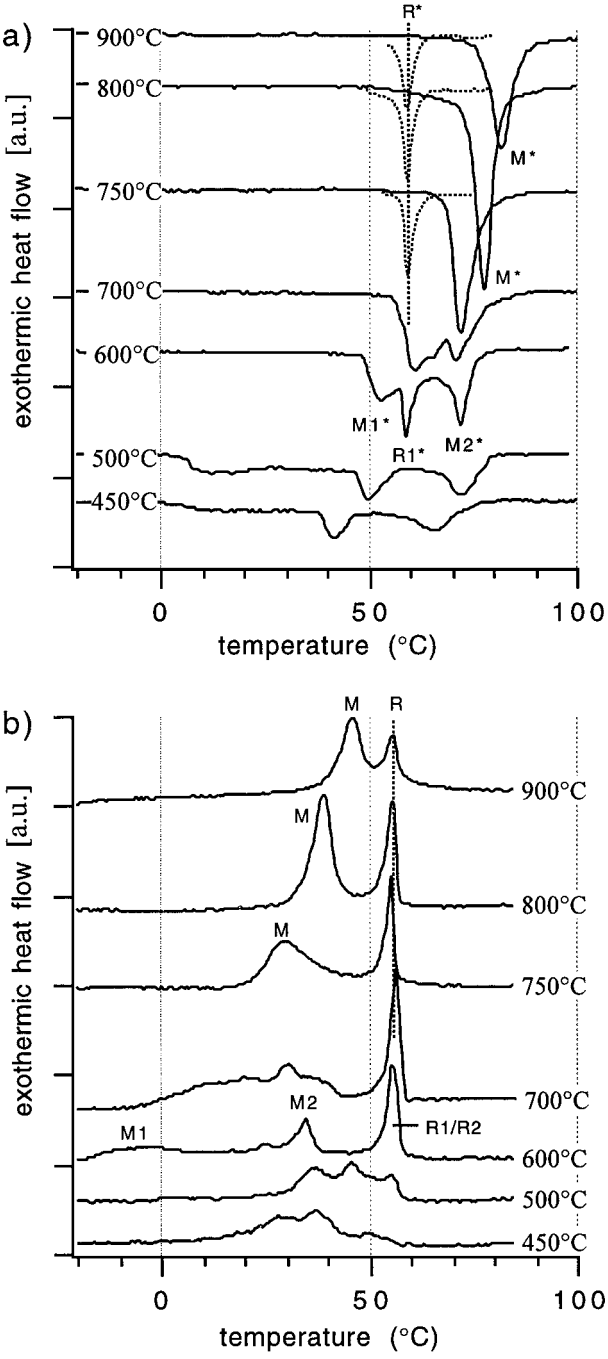

Figure 2 DSC heating (a) and cooling (b) curves as a function of annealing temperature ($t = 30$ min, water-quenched, 50.4 at.% Ti).

and cooling curves. For example, the sample was cooled from 100°C to 50°C, i.e. a temperature just below the peak R1/R2 in Fig. 2b. By subsequent heating, the corresponding peak R1* in the DSC heating curve of Fig. 2a could be identified. These two peaks are considered to be related to an austenite/R-phase transformation because of the small transformation hysteresis of 3.5 ± 0.5°C. A more detailed consideration suggested that in this sample two zones with different transformation behavior can be distinguished. At $T > 80$°C the whole film is in the austenitic phase. When cooled down, both zones transform to the R-phase at the same temperature, i.e. at 56°C (peak R1/R2 in Fig. 2b). However, both zones transform to the martensitic phase at different temperatures and over a relatively wide range (peak M2 and relative maximum M1). During heating, only zone 1 retransforms to the austenitic state via an R-phase (peaks M1* and R1* in Fig. 2a). Zone 2 retransforms directly from martensite to austenite at a somewhat higher temperature (peak M2* in Fig. 2a). The transformation behavior of the sample annealed at 700°C can be interpreted in principle in a similar way. The investigation is not straightforward in this case, because several peaks of zone 1 and 2 merged.

TABLE I Phase transformation temperatures as a function of annealing temperature (see Fig. 2)

T (°C) (annealing)	M^* (°C)	R^* (°C)	M (°C)	R (°C)
$600 \leq T \leq 700$	–	60	–	56
750	72	60	29	57
800	78	59	39	56
900	82	59	46	56

Annealing at temperatures in the range from 750°C to 900°C results in more clearly defined DSC peaks. During heating, a single peak appears (full line in Fig. 2a, peak M*). This indicates a more uniform phase transformation. The transformation enthalpy of 22 ± 3 J/g confirms that this peak is related to a direct transformation from martensite to austenite. Table I summarizes transformation temperatures of these samples. Peak M* shifts by +10°C when the annealing temperature is raised from 750°C to 900°C. In the DSC cooling curves two distinct peaks were recorded. The R peak at 56 ± 1°C could already be identified at lower annealing temperatures (enthalpy $H_R = 6.5 \pm 1$ J/g). Its position is independent of the annealing temperature. The second peak (labeled M, enthalpy $H_M = 11 \pm 1$ J/g) corresponds to the transformation of the R-phase to martensite. This peak becomes narrower with increasing annealing temperature and shifts by +17°C. The hysteresis M/M* of the martensitic transformation decreases slightly from 43°C to 36°C.

After partial cycling (cooling down just below the R peak and heating up again), the R-phase/austenite transformation (R* peak, enthalpy $H_{R*} = 5.5 \pm 0.5$ J/g) can be displayed in the heating curves, instead of the martensite/austenite transformation (M* peak). The R* peaks are indicated by dashed lines in Fig. 2a. They can also be considered as independent of annealing temperature. The R/R* hysteresis remains unchanged.

All samples annealed between 450°C to 900°C have metallic ductility and show a one-way shape memory effect when heated above their transformation temperature.

4.2. TEM investigation of the microstructure

4.2.1. Grain structure

The evolution of the microstructure as a function of annealing temperature in the above described samples was investigated by TEM (Philips CM 20, 200 kV). Samples were prepared by ion milling for several hours (Gatan DuoMill, 5 kV, 14°, Ar). They were heated *in situ* to about 100°C during the observations, i.e. they were in the austenitic phase. Fig. 3 shows a typical bright-field image of the film annealed at 450°C for 30 min. Its overall microstructure is particularly inhomogeneous.

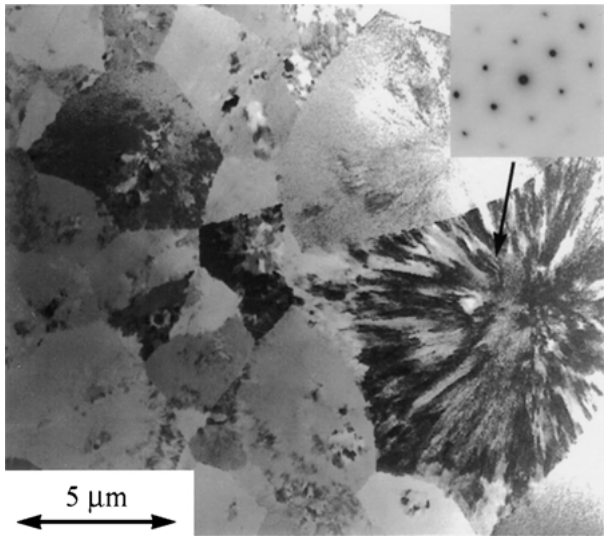

Figure 3 Microstructure of a film annealed at 450°C for 30 min. "Normal" grains with coexisting uniform and heterogeneous zones are visible. The diffraction pattern taken in the spherulites corresponds to the [1,1,1] zone axis of the cubic B2 austenitic phase.

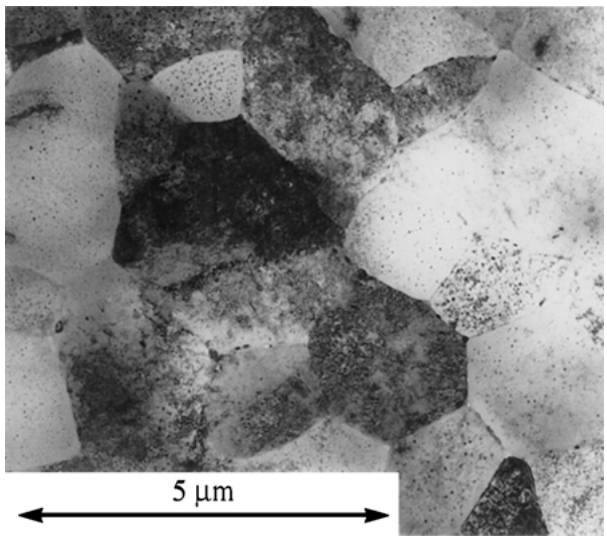

Figure 4 Microstructure of a film annealed at 800°C for 30 min.

Most of the grains are 1.5 to 4.5 μm in diameter and possess coexisting uniform and more heterogeneous zones. Larger grains extending up to 15 μm appear also rather frequently. This type (indicated by an arrow in Fig. 3) has a very specific internal microstructure with a spherulitic crystalline growth symmetry. Selected area diffraction (SAD) patterns, covering a large part of such a grain, correspond to a monocrystalline austenitic structure (see inset of Fig. 3, camera length $L = 0.5$ m). This indicates that the orientation of zones with different contrast in the interior of the grain vary only by a very small angle.

In the film annealed at 600°C for 30 min, the big spherulites do not appear (micrograph not shown). A rather non-uniform bimodal grain size distribution with a typical size varying between 1.5 to 3.0 μm and zones with somewhat larger grains in the range from 3 to 6 μm is observed. Fig. 4 is a bright field image of a film sample annealed at 800°C for 30 min. The grain size ranges from 1 to 2.5 μm and the distribution becomes more uniform with increasing annealing temperature. Grains with larger diameter do not appear in samples annealed at 800°C or 900°C.

4.2.2. Precipitates

In the samples annealed at 450°C a small amount of precipitates was formed at the grain boundaries. A TEM micrograph is shown in Fig. 5. These precipitates have oval shape with a maximum length of 40 to 50 nm. They were too small to be identified by SAD but they are most likely identical to the Ti_2Ni precipitates found at the grain boundaries in samples annealed at higher temperatures (see Fig. 8). No precipitates are visible in the interior of the grains. In some diffraction patterns weak streaks were observed. Such streaks were reported to be related to the presence of Guinier-Preston zones in Ti rich films, which may appear after annealing at relatively low temperatures [15].

The micrograph in Fig. 6 shows a grain in a film annealed at 600°C for 30 min. The most striking observation is the appearance of a large amount of small round-shaped precipitates with a diameter of 20 to 30 nm in the interior of the grains. Their distribution is homogeneous. A comparable microstructure was observed

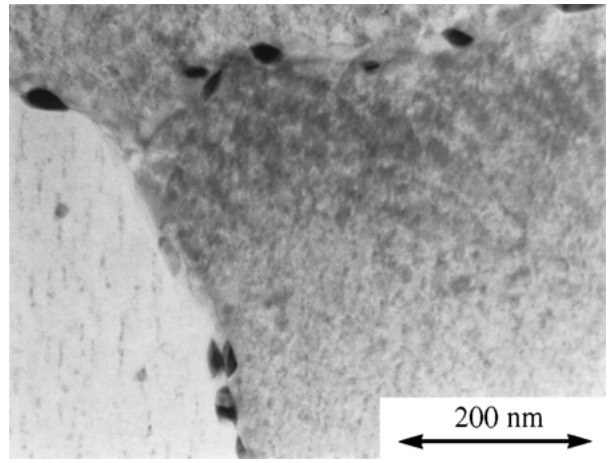

Figure 5 Small precipitates at the grain boundaries in the film annealed at 450°C for 30 min (water-quenched, 50.4 at.% Ti).

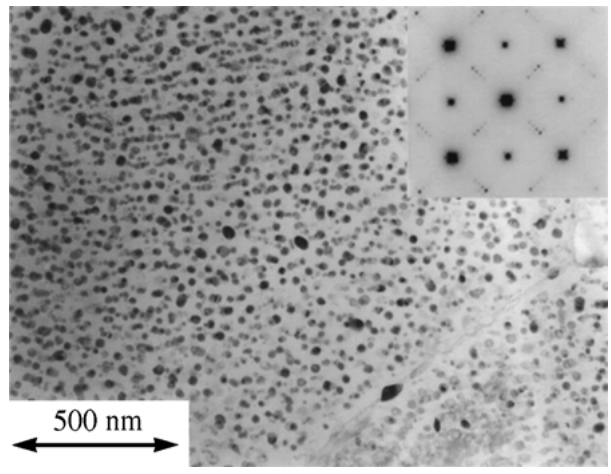

Figure 6 Film annealed at 600°C for 30 min. Grain with a dense distribution of round Ti_2Ni precipitates in the interior. The diffraction pattern corresponds to an austenite [1,0,0] zone axis superposed on a pattern generated by Ti_2Ni particles with the same orientation (water-quenched, 50.4 at.% Ti).

previously by other authors after annealing a Ti rich film in the same temperature range but for a longer time [19]. A small depleted zone with a maximum width of 50 nm is observed in the grains near the grain boundary. Precipitates at the grain boundaries have approximately doubled in size compared to the sample annealed at 450°C. The round precipitates in the grains could be identified as Ti_2Ni. A typical SAD pattern is shown in the inset of Fig. 6 ($L = 1$ m). As pointed out by Ishida *et al*. [15], this pattern corresponds to the [1,0,0] zone axis of the cubic austenitic matrix superposed on a pattern generated by Ti_2Ni particles having the same orientation as the matrix. Ti_2Ni was reported to have an fcc structure with a lattice parameter that is about four times larger than that of Ni-Ti [16]. Being located very close to the Ni-Ti spots in the diffraction pattern, the Ti_2Ni spots are hardly visible. Groups of smaller spots are mainly related to double diffractions [15]. This orientation relationship between the Ni-Ti matrix and these precipitates was observed in different zone axes of the Ni-Ti matrix. Annealing at 700°C for 30 min does not change significantly the microstructure.

The density of the round precipitates tends to decrease and the width of the depleted zone increases, after annealing at 750°C or 800°C for 30 min. It was suggested previously that this type of Ti_2Ni precipitates in the interior of the grains may represent a thermally unstable microstructure [19]. The diffraction pattern generated by the Ti_2Ni precipitates is only very weak after annealing at 750°C and vanishes in the background signal after annealing at 800°C, despite of the non-negligible amount of precipitates in the grains (see in Fig. 7, $L = 1$ m). High resolution electron microscopy (HREM) indicates however, that there exists still an at least partial coherency between the precipitates and the matrix.

Fig. 8 is a micrograph of a grain after annealing at 900°C for 30 min. The amount of precipitates in the grains has strongly reduced, none at all or only a very small number are present in the center region of the grains. Their average diameter has slightly increased to about 30 to 40 nm. The precipitates at the grain boundaries are much bigger compared to the samples annealed at lower temperatures. The typical size varies between 150 and 250 nm, oval shaped ones may extend to a length of 400 nm. These precipitates could also be identified as Ti_2Ni (inset in Fig. 8, $L = 0.5$ m).

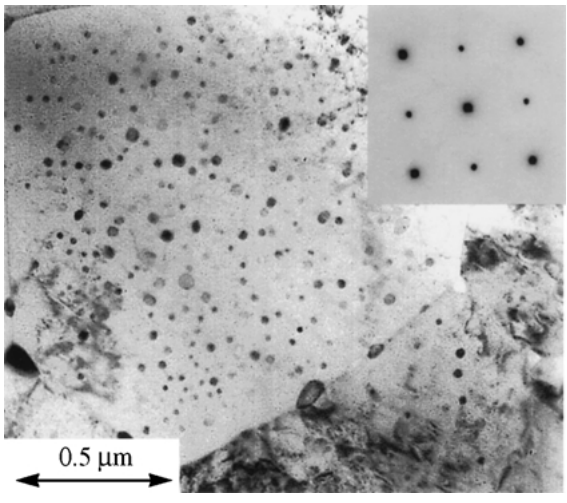

Figure 7 Film annealed at 800°C for 30 min. Grain with round Ti_2Ni precipitates in the interior. The diffraction pattern corresponds to an austenite [1,0,0] zone axis. The Ti_2Ni pattern vanishes in the background signal (water-quenched, 50.4 at.% Ti).

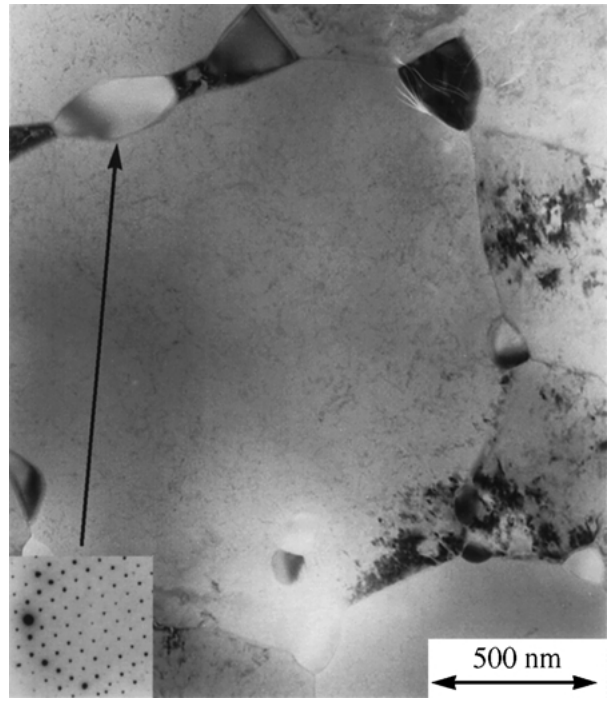

Figure 8 Film annealed at 900°C for 30 min. Grain with big Ti_2Ni precipitates at the boundaries. The diffraction pattern corresponds to the [1,0,1] zone axes of Ti_2Ni (water-quenched, 50.4 at.% Ti).

4.3. Discussion

The presence of spherulites (Fig. 3) is due to a fast grain growth around nucleation sites, such as impurities or locally enhanced stress fields, at the very first stage of the crystallization of the initially amorphous material. This idea is supported by an observation made in Ni-Ti films annealed by a localized laser spot, where isolated round austenite grains, embedded in the amorphous matrix, were found at the amorphous/crystalline interface [6]. The very broad transformation range in the DSC curves of films annealed at 450°C and 500°C is attributed to their heterogeneous microstructure.

The DSC curves for 600°C and 700°C reflect multiple transformations at different temperatures. At least two zones with different transformation behavior could be distinguished (Fig. 2). The corresponding micrographs revealed that the large amount of Ti_2Ni precipitates inside the grains may play a non-negligible role (Fig. 6). Preliminary TEM *in situ* observations of the martensitic transformation inside the grains indicate that these precipitates seem to hinder the propagation of martensitic plates. Stress fields around these coherent particles and/or local variations of the matrix composition in the vicinity of the precipitates are possible reasons for local transformation temperature shifts. However, more detailed *in situ* observations will be necessary in order to determine with certainty to what extent the grain boundaries itself, the depleted zones or the precipitates contribute to this particular transformation behavior.

The continuous shift of the M and M* peaks in Fig. 2 after annealing in the temperature range from 750°C to 900°C may be, at least partly, related to a slight composition shift of the Ni-Ti matrix itself. On the one hand, the solubility of Ti in the Ni-Ti matrix increases. The NiTi-Ti_2Ni phase boundary shifts by about 0.2 at.% to the Ti rich side in this temperature range [17]. However, the effect on the transformation temperatures in a Ti rich martix has not been clearly investigated yet. On the other hand, enhanced diffusion of excess Ti to the grain boundaries can counterbalance this effect. The limited accuracy of composition measurements in the interior of grains with precipitates makes quantitative evaluations difficult. The decreasing amount of round Ti_2Ni precipitates in the grains may also play a role.

Gyubo *et al.* [18] distinguish three clearly defined cases for Ni-Ti films annealed at different temperatures, characterized by the possible occurrence of an R-phase. In our case, we demonstrate a more complex, multiple transformation behavior in the temperature range up to 700°C. It should be pointed out that, because of different fabrication and annealing parameters, a thorough comparison of the results obtained by different authors is not straightforward and requires also a detailed comparison of the film microstructure.

5. Film characterization as a function of annealing time

5.1. DSC curves

The transformation properties were also studied as a function of annealing time (same film as in Section 4). Annealing was carried out at 700°C for 10 min up to 3 h (water-quenched). The DSC curves are shown in Fig. 9. These samples possess metallic ductility and a shape memory effect. After annealing for 10 min, the DSC heating curve showed a wide-spread multiple transformation with several relatively weak peaks. This structure is similar but stronger pronounced after annealing for 30 min (DCS curves for 700°C/30 min are identical in Figs 2 and 9). Transformation peaks related to two different zones could be distinguished (see discussion in Section 4, sample annealed at 600°C/30 min). The dashed lines in the DSC curves display a martensite/R-phase transformation obtained by partial thermal cycling (R*-peak).

Increasing the annealing time to 1 h and 3 h results in better defined uniform transformations. In the DSC heating curves a single martensite/austenite transformation peak M* appears. It becomes sharper for longer annealing time, as well as the M peak in the cooling curve, but the peak maximum does not shift significantly. The position of the R* and the R peaks also remains constant.

5.2. Grain structure and precipitates

No significant difference in grain size or size distribution can be observed by comparing samples annealed for 10 min and for 3 h at 700°C. The grains itself are homogeneous with a typical size in the range from 2 to 4 μm. A similar observation was reported by other authors after annealing a Ti rich film at the same temperature but for a longer time (1 h to 100 h) [19]. The

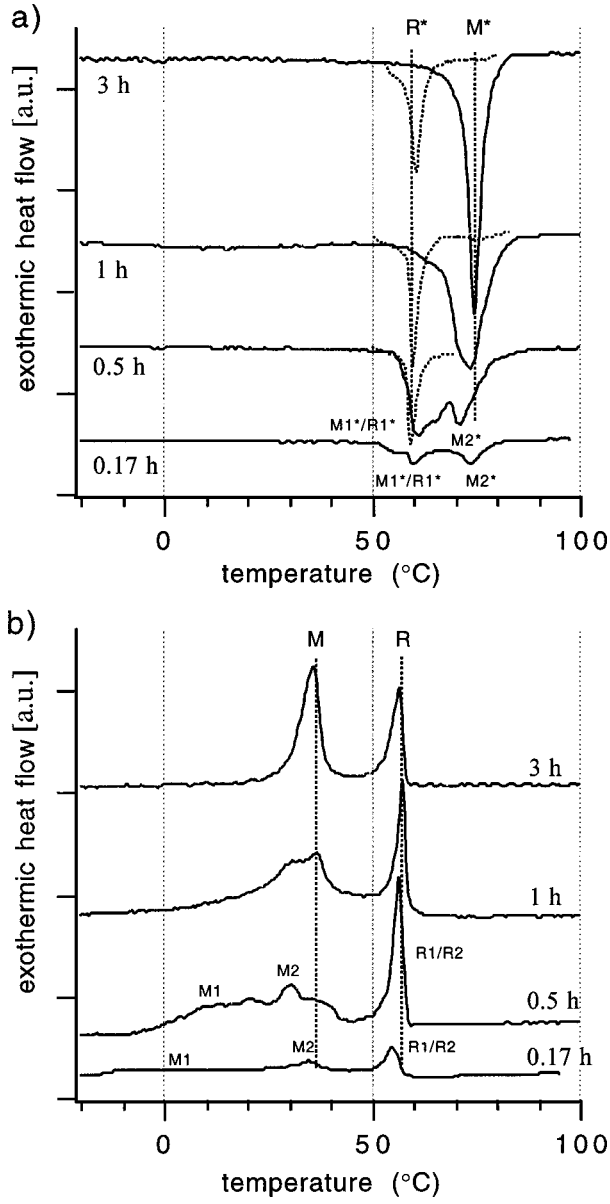

Figure 9 DSC heating (a) and cooling (b) curves as a function of annealing time ($T = 700$°C, water-quenched, 50.4 at.% Ti).

phenomenon was attributed to a pinning effect of Ti_2Ni precipitates at the grain boundaries. Our results reveal, however, that the grain growth seems to be accomplished already after a much shorter time.

The micrograph shown in Fig. 10 displays that precipitates inside the grains (diameter of 10 to 30 nm) and at the grain boundaries (length up to 100 nm) are already present after annealing for 10 min at 700°C. The SAD pattern in Fig. 10 ($L = 1$ m) demonstrates an at least partial coherency of the precipitates in the grains and the matrix, as observed before in Fig. 6. Micrographs taken after annealing for 3 h (not shown) reveal that the distribution of precipitates in the grains is not strongly affected by annealing in this time range. Nevertheless, their amount tends to decrease. The intensity of the SAD signal generated by the Ti_2Ni particles weakens and vanished in the background after annealing for 3 h.

5.3. Discussion

M and M* peaks shifted to higher temperatures for increasing annealing temperature but their position

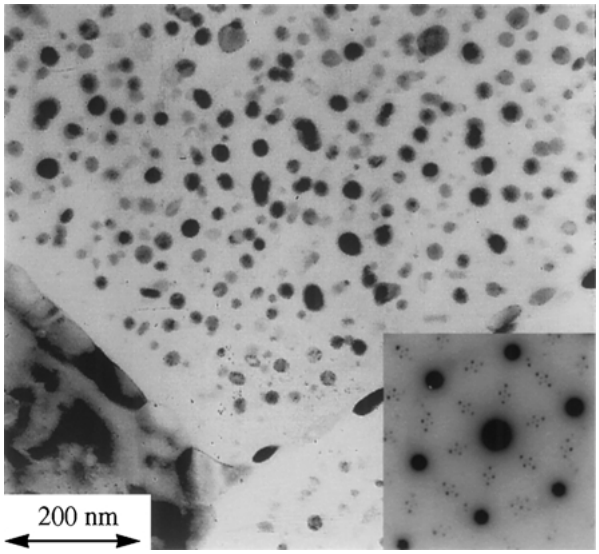

Figure 10 Ti_2Ni precipitates in the grains and at the boundaries of the film annealed at 700°C for 10 min. The diffraction pattern corresponds to an austenite [1,1,1] zone axis. It is superposed on a pattern of Ti_2Ni particles with the same orientation (water-quenched, 50.4 at.% Ti).

remains nearly constant when the annealing time is varied. These observations suggest that diffusion of Ti and the distribution of Ti rich precipitates in the grains are stronger affected by the annealing temperature than by the annealing time. This is in agreement with the micrographs of the corresponding samples. In addition to that, the solubility of Ti in the matrix is constant under isothermal conditions, so no shift of the transformation temperatures is expected due to this effect. The sharpening of M and M* peaks for longer annealing time can be attributed to the progressing homogenization and relaxation of the matrix for example in zones around the Ti_2Ni precipitates in the grains or at the grain boundaries.

6. Deposition on hot substrates

A series of experiments was carried out to study the effect of the substrate temperature during deposition on the microstructure of the films. The films investigated in this context have been deposited on Si/SiO_2 substrates by co-sputtering a pure Ni-Ti target (material I, RF 5.1 W/cm^2) and a pure Ti target (RF 1.4 W/cm^2).

The microstucture of such a film (thickness 5 μm, equiatomic composition) deposited on an unheated substrate and subsequent furnace annealing at 500°C for 30 min is comparable to the result shown in Section 4 (see Fig. 3). It is non-uniform, comprising spherulitic and "normal" grains with coexisting granular and uniform zones.

Films were deposited on substrates heated to 300°C and 450°C, respectively. The as-deposited films are amorphous. The microstructure of these films after subsequent furnace annealing at 500°C for 30 min is also very heterogeneous.

An important change occurred when the substrates were heated to 530 ± 20°C during deposition. The resulting as-deposited film is crystalline. Its microstructure is shown in Fig. 11. In contrast to previous samples, this film has a very uniform distribution of small crystallites. The average grain size is 200 nm. Larger

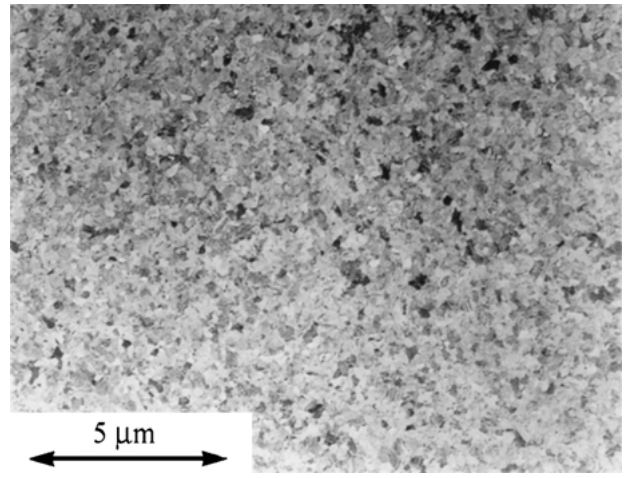

Figure 11 Microstructure of a film deposited on a substrate heated to 530 ± 20°C (crystallized during deposition, no subsequent annealing).

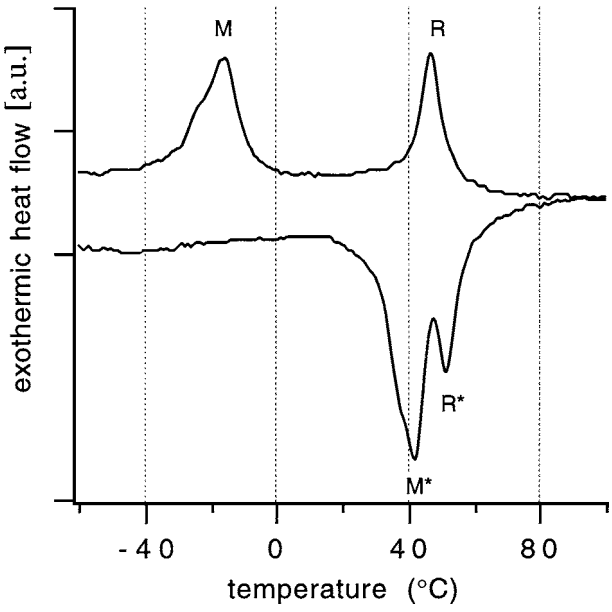

Figure 12 DSC curves of a film crystallized during deposition.

grains do not appear in this film. The corresponding DSC curves are displayed in Fig. 12 (scale enhanced by about a factor of 5 with respect to Figs 2 and 9). A phase transformation via an R-phase occurs during heating and cooling. Peaks are well-defined but very small and comparable in amplitude with samples annealed near the crystallization temperature or for very short time.

7. Variation of the film composition

7.1. DSC curves

The average amount of Ti in the films was enhanced by incorporating an increasing number of Ti pellets in the targets (material II, 50.5 at.% Ti, RF 6.1 W/cm^2, thickness 8 μm). All films of this series were annealed identically at 800°C for 30 min in a vacuum furnace and furnace cooled (heating rate 600°C/h, during cooling the temperature decreases from 800°C to 500°C in 2 min and then at a slower rate). The resulting DSC curves are shown in Fig. 13a and b. For each deposition, new targets were employed and small film samples (about 60 mm^2) were taken from the same substrate

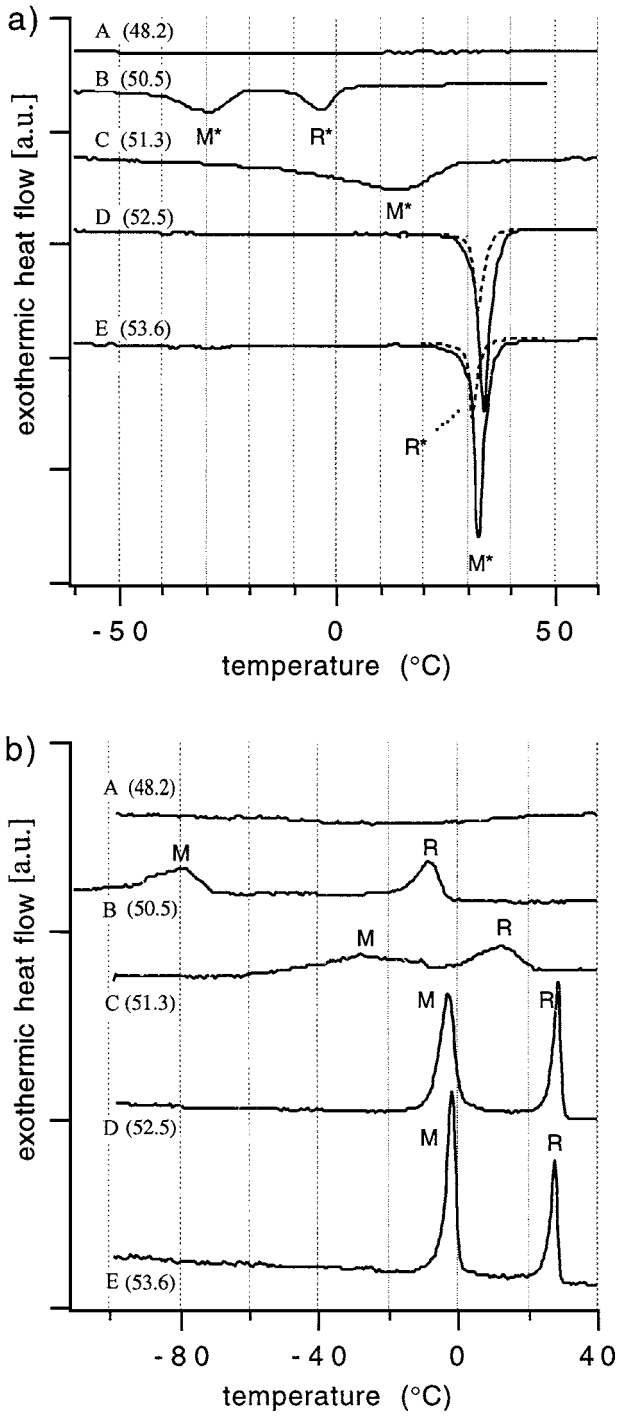

Figure 13 DSC heating (a) and cooling (b) curves as a function of film composition (at.% Ti in parenthesis, annealed at 800°C for 30 min, furnace-cooled).

position in order to avoid possible effects of target erosion or slightly non-uniform deposition.

The results are summarized in Table II. Sample A (48.2 at.% Ti, co-sputtered with two pure Ni-Ti targets) did not transform in the investigated temperature range. Adding two Ti pellets in each target raises the amount of Ti in the film to 50.5 at.% (sample B). Small DSC peaks of a martensite/R-phase (M/M*) and an R-phase/austenite (R/R*) transformation appear below 0°C. Sample C (51.3 at.% Ti) still shows small and strongly broadened DSC peaks but shifted to higher temperatures. The M* and R* peaks merge to a single broad peak in the DSC cooling curve. This corresponds to a shift of about +44°C for the M* peak and about +17°C for the R* peak.

The DSC curves of sample D (52.5 at.% Ti) show distinct peaks that shifted by about 20 ± 3°C to higher temperatures compared to sample C. The martensite transforms directly to austenite during heating (M* peak, solid line in Fig. 13a). The R* peak is resolved by partial cycling (dashed line in Fig. 13a). In the cooling curve the R peak and M peak are clearly separated. Adding more than 3 Ti pellets to the targets did not change the transformation behavior in a significant way (sample E, 5 incorporated Ti pellets, 53.6 at.% Ti).

7.2. Film microstructure

The microstructure of samples A to E was investigated by TEM observations (heated *in situ* to about 100°C). Fig. 14 shows a typical grain structure of sample A. The average grain size is in the range of 0.5 to 1.5 μm. SAD patterns show that the matrix is in the austenitic phase. In the interior of the grains a large amount of homogeneously distributed lenticular precipitates are present (100 to 250 nm long, maximum width of about 50 nm). These precipitates have been identified as Ni_4Ti_3. They have a defined orientation relationship with the Ni-Ti matrix as can be deduced from the SAD pattern shown in Fig 14a ($L = 0.5$ m). Relatively broad and indistinct contrast fields around the precipitates indicate the existence of stress fields due to the at least partial coherency of these precipitates with the matrix. A second type of precipitate was also present in this film (diameters of 150 to 200 nm). They were found mainly at the grain boundaries, especially at triple points. Diffraction patterns of these precipitates correspond to Ti_2Ni (see Fig. 14b, $L = 0.5$ m).

TABLE II Transformation temperatures and enthalpies H as a function of film composition (see Fig. 13, annealing at 800°C for 30 min, furnace-cooled)

Sample	A	B	C	D	E
Ti pellets target 1/2	0/0	2/2	2/3	3/3	5/5
at.% Ti	48.2	50.5	51.3	52.5	53.6
M^* (°C)	–	-30 ± 3	14 ± 5	34	33
H_{M^*} (J/g)	–	7.0 ± 0.5	15 ± 1	20.0 ± 0.5	18.4 ± 0.5
R^* (°C)	–	-3 ± 2	–	32	31
H_{R^*} (J/g)	–	4.2 ± 0.5	–	6.4 ± 0.5	5.4 ± 0.5
M (°C)	–	-80 ± 10	-25 ± 10	-2	-1
H_M (J/g)	–	6.7 ± 0.5	9.8 ± 1.0	11.0 ± 0.5	10.6 ± 0.5
R (°C)	–	-7	12 ± 5	29	28
H_R (J/g)	–	5.7 ± 0.5	4.6 ± 1.0	6.6 ± 0.5	5.5 ± 0.5

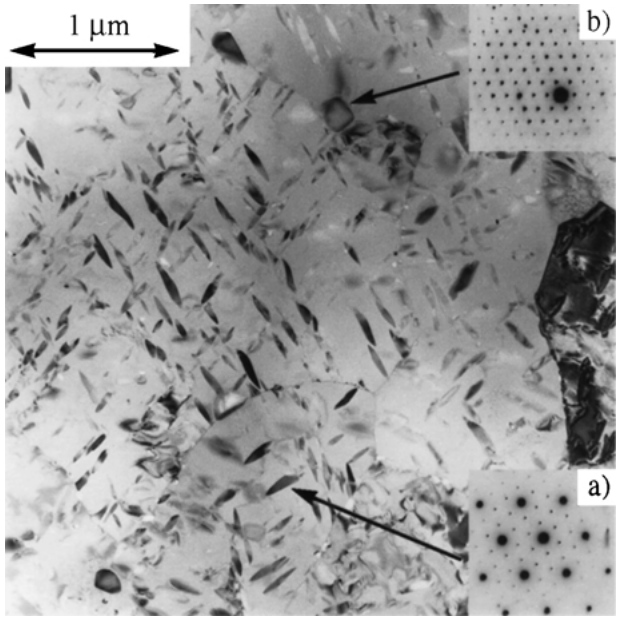

Figure 14 Precipitates in a grain of sample A. The diffraction pattern (a) corresponds to a superposition of the [1,1,1] Ni-Ti austenite axis and the [−1,−1,−1] zone axis of Ni_4Ti_3. Pattern (b) taken in a precipitate at the grain boundary is the [1,0,1] zone axis of Ti_2Ni (48.2 at.% Ti, 800°C/30 min, furnace-cooled).

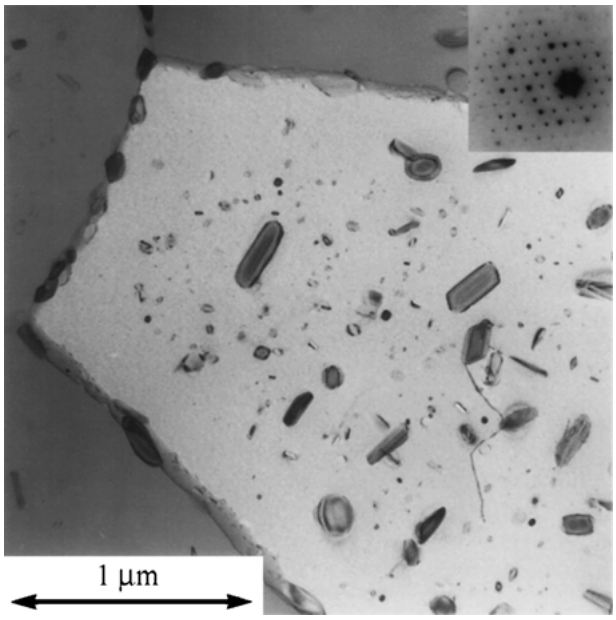

Figure 15 Precipitates in a grain of film sample B. The diffraction patterns taken in the larger precipitates correspond to Ti_2Ni. The inset shows a [1,0,1] zone axis (50.5 at.% Ti, 800°C/30 min, furnace-cooled).

Increasing the amount of Ti in the film has strong effect on its microstructure. Fig. 15 shows a grain of film sample B. The grain size is typically in the range from 3.5 to 7.5 μm, that means the average grain size increased by more than a factor of 5 compared to the previous sample, despite the same annealing process. In this film comparatively large Ti_2Ni precipitates appear in the grains. They have been identified by SAD (see inset of Fig. 15, $L = 0.5$ m) and EDS. In contrast to the very small round-shaped Ti_2Ni precipitates in the interior of the grains observed in the samples of Sections 4 and 5, these particles are more or less plate-shaped and differently orientated. Their length varies typically

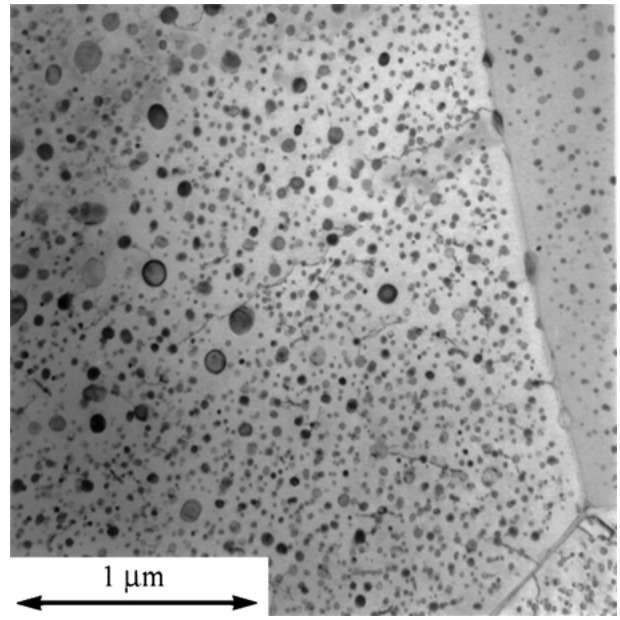

Figure 16 Round Ti_2Ni precipitates in a grain of sample D (52.5 at.% Ti, 800°C/30 min, furnace-cooled).

within a range of 100 nm to 300 nm with a thickness of about 20 nm for the largest precipitates. The amount of precipitates in this film with a nearly equiatomic composition is relatively low. No contrast changes due to stress fields can be found. A certain amount of much smaller (diameter 20 to 40 nm), but not identified precipitates, is also present in the interior of the grains. Ti_2Ni precipitates with a typical length between 70 and 220 nm are present at the grain boundaries. The microstructure of sample C is very similar, but the density of the small precipitates in the grains increased.

The microstructure of a grain of sample D, shown in Fig. 16, looks similar to the films annealed at 600°C to 800°C investigated in Section 4 (Figs 6 and 7). A dense distribution of round Ti_2Ni precipitates appears in the grains. The mean diameter is about 20 nm near the grain boundaries. This value is comparable to that measured in the previous samples. In the center region of the grains these precipitates may become much larger with diameters up to 120 nm. The amount of Ti_2Ni precipitates at the grain boundaries is relatively small. They have a maximum length of about 150 nm. The typical grain size in this film varies between 4 to 7 μm which is comparable to sample B. A further increase of the Ti amount in the film has again an important effect on the film microstructure. A representative grain of film sample E is shown in Fig. 17. The typical grain size in this film is 1.5 to 3 μm, i.e. grains are by a factor of 2 smaller than in samples B and D. The amount of larger Ti_2Ni precipitates in the grains increases as well as their maximum size (up to 200 nm). The most striking effect compared to sample D is the presence of many big Ti_2Ni precipitates at the grain boundaries. They may attain diameters up to 0.4 μm. Big precipitates at the grain boundaries and relatively small grain size have already been found in a film annealed at 900°C shown in Fig. 8. Together with the present sample, these observations confirm the previously mentioned pinning effect of such precipitates at the grain boundaries [19].

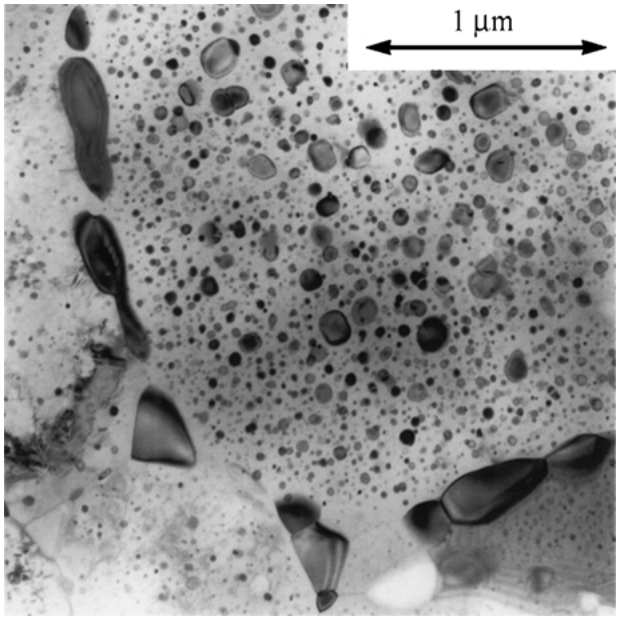

Figure 17 Sample E: Round Ti_2Ni precipitates in the interior of a grain and large Ti_2Ni precipitates at the grain boundaries (53.6 at.% Ti, 800°C/30 min, furnace-cooled).

7.3. Discussion

A detailed study of plate-shaped Ni_4Ti_3 precipitates in thin Ni-Ti foils, such as observed in sample A, has been carried out previously by other authors [20]. Similar precipitates have also been investigated in Ni rich Ni-Ti wires and thin films [21, 22]. Stress fields around these coherent precipitates have been reported to have great influence on the transformation behavior and the DSC curves of the films [21]. The important volume fraction occupied by the Ni_4Ti_3 precipitates in the Ni-Ti matrix of sample A combined with high stress fields is probably the reason why no martensitic transformation occurs in this case. Following an investigation presented by other authors, Ni rich precipitates should not appear after annealing at 800°C for 30 min in a material with 48 at.% Ti [23]. In the present case, the sample has not been water-quenched, so Ni rich precipitates may have formed during heating up to 800°C or cooling down to room temperature.

A surprising phenomenon is the co-existence of Ni rich precipitates and Ti rich precipitates in sample A. A similar observation was made in Ni rich Ni-Ti wires [24]. In this case, Ti rich precipitates were supposed to have formed already during the fabrication of the raw material, whereas Ni rich precipitates were formed during subsequent annealing. The inhomogeneous sputter target composition with incorporated pure Ti pellets may be the origin of Ti agglomerates and Ti rich precipitates in the investigated film, despite of an average Ni rich composition.

M/M* and R/R* peaks appear and shift to higher temperatures in sample B and C. This is probably directly related to the increase of the amount of Ti in the matrix of the films. However, their position in sample D and E are not affected anymore by an increase in the amount of Ti in the sputter targets. The corresponding micrograph shows that excess Ti atoms are mainly absorbed at the grain boundaries (Fig. 17). These precipitates do not deteriorate the transformation behavior of the films. It is expected that the composition of the Ni-Ti matrix is the same in both samples. The well-defined and sharp DSC peaks suggest that the matrix between the big Ti_2Ni precipitates inside the grains is quite homogeneous.

The DSC curves in Fig. 13 should also be compared to those shown before in Fig. 2. Samples D and E have up to 3 at.% Ti more than the film investigated in Sections 4 and 5. Nevertheless, the transformation temperatures are significantly lower. Possible explanations are an influence of the annealing process (water-quenched or furnace cooled), a slight contamination of the target material (material II) or the dense distribution of relatively big Ti_2Ni precipitates in the interior of the grains.

An investigation of transformation temperatures in Ni-Ti films as a function of composition was carried out previously by Gyobu *et al*. [18]. A detailed comparison reveals differences in the transformation behavior and temperatures. In sample B, for example, Gyubo *et al*. would expect a single-stage transformation, whereas a two-stage transformation via an R-phase occurs in our case. For higher Ti content, we observe qualitatively the same transformation behavior (one-stage during heating, two-stage during cooling). However, the R-peak, which remains constant for all Ti rich films in the above quoted work (for annealing at 500°C/1 h), shifts to higher temperatures in our experiments (sample B, C and D). A similar statement can be made for the M/M* peaks (for annealing at 800°C), but the quite complex evolution of these peaks as a function of annealing temperature and film composition makes a more detailed comparison between the two papers very difficult. As mentioned before, an investigation of the microstructure would always be necessary, in order to understand deviations in the transformation behavior of films produced by different groups.

8. Conclusion

DSC measurements allow for a systematic investigation of the effect of annealing parameters on the transformation behavior of Ni-Ti sputter-deposited thin films. These observations were related to modifications of the film microstructure. After annealing near the crystallization temperature, the films have a very heterogeneous internal structure. This results in DSC curves showing multiple transformations extending over a broad temperature range. The very dense distribution of small round and coherent Ti_2Ni precipitates appearing at higher annealing temperatures has a non-negligible influence on the transformation behavior. DSC curves show very well defined transformation peaks after annealing at 800 or 900°C where round Ti_2Ni particles in the interior of the grains have almost disappeared. Large Ti_2Ni precipitates, that have formed at the grain boundaries in the later case, have no evident influence on the transformation behavior but may limit the grain growth. Annealing for only 10 min at 700°C is not sufficient to obtain a well transforming film. A dense distribution of Ti_2Ni coherent precipitates was already present in the grains of this film. Increasing the annealing time had only a weak effect on the film microstructure. Nevertheless there is a clear evolution in the DSC curves.

These experiments showed that the transformation behavior of the martensite is very sensitive to slight modifications of the Ti_2Ni precipitates in the interior of the grains in the lower annealing temperature range and for relatively short annealing times. On the other hand, it turned out that the R-phase transformation is very insensitive with respect to annealing parameters and microstructure of the films.

Films deposited on substrates heated above 500°C crystallize during deposition with a granular microstructure composed of grains with a typical diameter of 200 nm. Transformation peaks are better defined than in amorphous as-deposited films that have been annealed at the same temperature.

By using Ti enriched sputter targets, the martensitic transformation temperatures could be shifted by over 60°C and the amount of precipitates in the films can be controlled. Big Ti_2Ni precipitates in the interior of the grains and at the grain boundaries, that form after annealing at 800°C in films with relatively large excess of Ti, do not deteriorate the transformation properties. In spite of the large volume fraction occupied by these precipitates, the DSC peaks are very well defined. The reminder of the matrix in these films appears to be less affected and more homogeneous than in films annealed at lower temperatures with a very dense distribution of small Ti_2Ni precipitates. By means of the presented fabrication method, films with a wide composition and transformation temperature range can be fabricated. The presented systematic investigation of the annealing parameters allows to design Ni-Ti shape memory films with suitable properties for various applications. The amount of precipitates can be controlled. Nevertheless, a more thorough physical understanding of the correlation between film microstructure and transformation behavior requires detailed *in situ* TEM investigations of the martensitic transformation.

Acknowledgements

The authors would like to thank Prof. F. Levy of the Institut de Physique de la Matière Complexe at the EPFL for placing his sputter deposition facilities at our disposal and H. Jotterand for technical support.

References

1. R. H. WOLF and A. H. HEUER, *J. MEMS* **4** (1995) 206.
2. A. D. JOHNSON and V. V. MARTYNOV, in Proc. SMST-97 (1997) p. 149.
3. L. BUCHAILLOT, S. NAKAMURA, Y. NAKAMURA, M. ATAKA and H. FUJITA, in Proc. SMST-97 (1997) p. 183.
4. K. IKUTA, in Proc. IEEE Int. Conf. on Robotics and Automation (1990) Vol. 3, p. 2156.
5. K. KURIBAYASHI and S. SHIMIZU, in Proc. Actuator 98 (Messe Bremen GmbH, Germany, 1998) p. 465.
6. Y. BELLOUARD, T. LEHNERT, J. E. BIDAUX, T. SIDLER, R. CLAVEL and R. GOTTHARDT, *Mat. Sci. Eng*. A **273–275** (1999) 795.
7. S. KAJIWARA, T. KIKUCHI, K. OGAWA, T. MATSUNAGA and S. MIYAZAKI, *Phil. Mag. Lett*. **74** (1996) 137.
8. S. MIYAZAKI and A. ISHIDA, *Mat. Sci. Eng*. A **273–275** (1999) 106.
9. E. SUKEDAI, T. KUNINORI, T. SHIRAISHI, T. ICHIKAWA and H. HASHIMOTO, in "Displacive Phase Transformations and Their Applications in Materials Engineering," edited by K. Inoue *et al*. (TMS, Warrendale, USA, 1998) p. 239.
10. S. CREVOISERAT, P. SCHERRER, T. LEHNERT, C. DIMITRIPOULOS and R. GOTTHARDT, in Proc. Int. Conf. On Solid-Solid Phase Transformations PTM 99 (Japan Institute of Metals, 1999) Vol. 12 p. 1064.
11. D. S. GRUMMON and T. J. PENCE, *Mat. Res. Soc. Symp. Proc*. **459** (1997) 331.
12. F. E. LUBORSKY, "Amorphous Metallic Alloys" (BMM Butterworth, 1983).
13. B. CLEMENS, *Phys. Rev*. B **33** (1986) 7615.
14. T. LEHNERT, S. TIXIER, P. BÖNI and R. GOTTHARDT, *Mat. Sci. Eng*. A **273–275** (1999) 713.
15. A. ISHIDA, K. OGAWA, M. SATO and S. MIYAZAKI, *Metal. Mat. Trans*. A **28** (1997) 1985.
16. M. MUELLER and H. KNOTT, *Trans. AIME* **227** (1963) 674.
17. G. F. BASTIN, G. D. RIECK, *Metall. Trans*. **5** (1974) 1817.
18. A. GYOBU, Y. KAWAMURA, H. HORIKAWA and T. SABURI, *Mater. Trans. JIM* **37** (1996) 697.
19. A. ISHIDA, M. SATO, A. TAKEI and S. MIYAZAK, *ibid.* **36** (1995)1349.
20. T. TADAKI, Y. NAKATA, K. SHIMIZU and K. OTSUKA, *Trans. Jap. Inst. Met*. **27** (1986) 731.
21. L. BATAILLARD and R. GOTTHARDT, *J. de Phys*. IV **5** (1995) C8-647.
22. A. ISHIDA, M. SATO, A. TAKEI, K. NOMURA and S. MIYAZAKI, *Metall. Mat. Trans*. A **27** (1996) 3753.
23. M. NISHIDA, C. WAYMAN and T. HONMA, *Met. Trans*. A **17** (1986) 1505.
24. L. BATAILLARD, Ph.D. thesis n°1518, Physics Department, EPFL Lausanne, Switzerland, 1996.

Received 23 April
and accepted 29 November 2001